Published in final edited form as:
J Neurosci. 2011 November 2; 31(44): 15983–15995. doi:10.1523/JNEUROSCI.3029-11.2011.

Opposing roles of voltage-gated Ca^{2+} channels in neuronal control of regenerative patterning

Dan Zhang, **John D. Chan**, **Taisaku Nogi**, and **Jonathan S. Marchant**[*]
Department of Pharmacology & The Stem Cell Institute, University of Minnesota Medical School, MN 55455, USA

Abstract

There is intense interest in developing methods to regulate proliferation and differentiation of stem cells into neuronal fates for the purposes of regenerative medicine. One way to do this is through *in vivo* pharmacological engineering using small molecules. However, a key challenge is identification of relevant signaling pathways and therein drugable targets to manipulate stem cell behaviour efficiently *in vivo*. Here, we use the planarian flatworm as a simple chemical-genetic screening model for nervous system regeneration to show that the isoquinoline drug praziquantel (PZQ) acts as a small molecule neurogenic to produce two-headed animals with integrated central nervous systems following regeneration. Characterization of the entire family of planarian voltage-operated Ca^{2+} channel alpha subunits ($Ca_v\alpha$), followed by *in vivo* RNAi of specific Ca_v subunits revealed that PZQ subverted regeneration by activation of a specific voltage-gated Ca^{2+} channel isoform (Ca 1A). PZQ-evoked Ca^{2+} v entry via Ca_v1A served to inhibit neuronally-derived Hedgehog signals, as evidenced by data showing that RNAi of Ca_v1A prevented PZQ-evoked bipolarity, Ca^{2+} entry and decreases in *wnt1* and *wnt11-5* levels. Surprisingly the action of PZQ was opposed by Ca^{2+} influx through a closely related neuronal Ca_v isoform (Ca_v1B), establishing a novel interplay between specific Ca_v1 channel isoforms, Ca^{2+} entry and neuronal Hedgehog signaling. These data map PZQ efficacy to specific neuronal Ca_v complexes *in vivo* and underscore that both activators (Ca_v1A) and inhibitors of Ca^{2+} influx (Ca_v1B) can act as small molecule neurogenics *in vivo* on account of the unique coupling of Ca^{2+} channels to neuronally-derived polarity cues.

Keywords

Ca^{2+} signaling; Ca^{2+} entry; stem cell; neurogenesis; disease

INTRODUCTION

Methods that generate large numbers of specific cell types as immunologically-matched replacements for diseased tissue have clear therapeutic potential, especially for neurodegenerative conditions. Three broad strategies that achieve this encompass protein-based approaches (growth factor 'cocktails'), genetic reprogramming (via specific transcription factors), and pharmacological engineering (small molecules that bias differentiation). While each method has advantages, the inherent appeal of small molecule based approaches translates to their potential for use *in vivo* with lesser risks than exogenous genetic reprogramming. Key challenges are identifying 'drugable' signaling pathways that regulate stem cell expansion and differentiation, and understanding the functional interplay of such pathways *in vivo*.

[*]**Corresponding Author**: march029@umn.edu, 612-624-4664 (T); 612-625-8408 (F) .

Ca^{2+} signaling exemplifies a well dissected pathway to nuclear reprogramming in differentiated neurons (Greer and Greenberg, 2008). In neural stem/progenitor cells also, *in vitro* screens have uncovered Ca^{2+} signaling modulators that regulate proliferation and adoption of neuronal cell fates (Diamandis et al, 2007; Schneider et al, 2008). While these insights derive from studying multipotent cells *in vitro*, it is important to discern whether similar principles hold *in vivo*. This is an important distinction as stem cell fate *in vivo* is controlled by cues inherent to the local microenvironment such that the efficacy of pharmacological agents identified *in vitro* will be modified by signals unique to the stem cell niche.

An attractive screening model for small molecule neurogenics is the planarian flatworm. Planarians exhibit impressive regenerative abilities owing to the maintained plasticity of their pluripotent stem cells ('neoblasts'), which differentiate into ~30 cell types during homeostasis and enforced tissue regeneration. These worms afford the opportunity to study regeneration of an entire nervous system by simple amputation assays, rather than simply the regrowth/repair of a single neuron (Newmark and Sanchez-Alvarado, 2002; Cebrià, 2007). Planarians hold great fascination for neuroscientists: they express a diverse array of neurotransmitters (Collins et al, 2010), occupy a unique evolutionary niche in terms of emergence of a centralized nervous system and have behavioral screening potential. Further, most planarian genes (~80%) show greater similarity to vertebrate orthologs relative to invertebrate sequences (Sánchez Alvarado et al, 2002; Fredlander et al, 2009).

Previously, while investigating the undefined mechanism of action of praziquantel (PZQ) – a drug used to treat Schistosomiasis - we found that PZQ subverted regeneration to produce viable, two-headed worms with integrated central nervous systems (Nogi et al, 2009). Initial data suggested PZQ miscued regeneration by modulating voltage-operated Ca^{2+} entry (Nogi et al, 2009). However, the lack of molecular information about voltage-operated Ca^{2+} channels (Ca_vs) in this system, precluded functional genetic testing of this hypothesis. Here, we define the planarian family of $Ca_v\alpha$ subunits and employ *in vivo* RNAi to show that PZQ subverts regeneration by selective activation of a $Ca_v\alpha$ isoform (Ca_v1A) to dysregulate neuronal Hedgehog signaling. This effect was opposed by another neuronal Ca_v1 isoform (Ca_v1B). These data support a unique interplay between specific Ca_v1 channels and neuronal Hedgehog signaling and justify analysis of Ca_v1 channels *in vivo* as targets for small molecule neurogenics and for PZQ, the mainstay therapeutic for treating a disease that infects 200 million people worldwide.

MATERIALS & METHODS

Worm husbandry

An asexual clonal GI strain (Gifu, Iruma river) of *Dugesia japonica* were maintained (~5,000 worms in 5L of water) at room temperature (20-23°C) and fed strained chicken liver puree (~10ml) once a week. Regenerative assays were performed using 5 day-starved worms in pH-buffered artificial water at 22°C (1x Montjuïch salts: 1.6mM NaCl, 1.0mM $CaCl_2$, 1.0mM $MgSO_4$, 0.1mM $MgCl_2$, 0.1mM KCl, 1.2mM $NaHCO_3$, pH 7.4 buffered with 1.5mM HEPES). Praziquantel (PZQ), sourced from Sigma (P4668) was used as a racemic mixture. The basic planarian methods used in these experiments are described in (Chan and Marchant, 2011).

In situ hybridization

Whole-mount *in situ* hybridization was performed at 55°C in hybridization solution (50% formamide, 5×SSC, 100μg/ml yeast tRNA, 100μg/ml heparin sodium salt, 0.1% Tween-20, 10mM DTT, 5% dextran sulfate sodium salt) incorporating digoxygenin (DIG)-labeled antisense riboprobe (40ng/ml) denatured at 72°C for 15 min prior to use (Nogi et al, 2009). A standard mixture of BCIP/NBT in chromogenic reaction solution was used for color development, followed by paraformaldehyde fixation. DIG-labeled antisense riboprobe was synthesized by RNA polymerase (Roche) from linearized pGEM-T Easy plasmid as the template. Probe regions were as follows: *PC2* (1-2285bp); *Hox9* (1-1491bp); *ndk* (122-1692bp); *nlg* (1-1204bp); *Inx7* (1-1528bp); *MHC* (4879-5905bp); *wnt1* (1-1162bp); *wnt11-5* (1-1050bp); *Hh* (59-1370bp from AB504739.1); *Ca_V1A* (1027-1865bp; 2229-4133); *Ca_V1B* (2722-4010bp; 4380-6059); *Ca_V2A* (120-962bp). Staining was resolved and archived using a Leica MZ16F stereomicroscope and a QiCAM 12-bit cooled color CCD camera.

Cloning strategies

Total RNA was isolated from 20 intact planarians using TRIzol® and cDNA subsequently synthesized using the SuperScript™ III First-Strand Synthesis System (Invitrogen). Novel $Ca_V\alpha$ cDNAs were identified by PCR amplification (LA Taq™ polymerase) using degenerative primers designed from regions with high sequence identity based on alignment with a published *Schistosoma mansoni* Ca_V1 sequence (Kohn et al, 2001b) and putative annotations in the *S. mansoni* (Berriman et al, 2009) and *Schmidtea mediterranea* genomes (Robb et al, 2008). Products were cloned into the pGEM®-T Easy vector (Promega) for sequencing. On the basis of initial sequence data, further sequence was predicted from genomic annotations and verified by screening either a cDNA library prepared from regenerating *D. japonica* fragments or freshly synthesized cDNA if not represented in the existing library. Final sequences of the Ca_V clones were assembled in pGEM-T Easy vector and resequenced three times. For RACE analysis, mRNA was separated and purified using Oligotex® mRNA mini Kits (Qiagen) and used to synthesize cDNA with gene-specific primers according to the manufacturer's instructions (5′/3′ RACE Kit, Roche). Oligo-dT primers were used to synthesize 3′RACE cDNA, and nested PCR to amplify 5′ RACE cDNA. Gene specific primers for RACE were: 5′RACE: *Ca_V1A* (5′CATTTTCTTCATCGCTGAGTTCGTCA-3, 5′-TTCTCCGCTAAGAACACCAAGAATTA-3′, 5′-TTGTTTCCTTGTGCATCATTTATCCA-3), *Ca_V1B* (5′-TCTGCATTGTTACCTTCTTCTTCTTC-3′, 5′-CGTTCAATAAGATGTAGTTTCCGCAA-3′, 5′-GACTTCATTCCAATCTTCACCAGTTAG-3′, 5′-GAGCAATGACTGCCAAAAACTATCAAA-3′); 3′RACE: *Ca_V1A* (5′-GGATTGGGAGCATTAGTTTCCTTGTA-3′, 5′-GGCTGCTGAAGACCCAATAAGAAC-3′, 5′-TATCTTCGTTGGTTTTGTCATCGTT-3′), *Ca_V1B* (5′-GCCTGGCTTATTATACAAATCAATCG-3′, 5′-TTACAGTGGCACATATAATAATCGACC-3′, 5′-GTTTTGTCATCGTTACGTTTCAGCA-3′). Products were gel purified (High Pure PCR Product Purification Kit, Roche) and fragments ligated into pGEM-T Easy vector for sequencing. A similar approach was used to isolate *D. japonica βcatenin-1*, *adenomatous polyposis coli* (*APC*), *hedgehog* (*Hh*), *patched* (*ptc*), *wnt1* and *wnt11-5*. Wnt nomenclature is from (Gurley et al, 2010). For *in vivo* RNAi, sequences were amplified using gene specific primers incorporating Kozak sequence and cloned into the IPTG-inducible vector pDONRdT7 using Gateway® BP Clonase (Invitrogen).

RNAi methods

In vivo RNAi was performed following a feeding protocol described previously (Nogi et al, 2009). Over several feeding/regeneration cycles, worms were fed a chicken liver and bovine red blood cell mixture containing transformed HT115 bacteria induced to express individual dsRNA constructs. Comparison of phenotypic scoring and drug effects were examined using paired t-tests, with differences considered significant at $p<0.05$ (*) and $p<0.01$ (**). All data are presented as mean ± standard error of the mean for the indicated number of experiments. As a control for non-specific RNAi effects, a *Schmidtea mediterranea six-1* (*Smed-six-1*) construct was used. This construct did not produce a phenotype in *D. japonica* regenerants, owing to nucleotide divergence between the *six-1* genes in the two planarian species. Targeted sequences were: *Ca_V1A* (1042-1831bp; 2229-4133bp), *Ca_V1B* (2722-4010bp; 4380-6059bp; 6194-7219bp), *Ca_V2A* (120-962bp), *βcatenin-1* (1-1351bp), *APC* (1-2413bp), *ptc* (95-2572bp), *Smed-six-1* (1-506bp). For assessment of knockdown following RNAi, cDNA from experimental cohorts of 10 worms, or from 40 posterior blastemas for *wnt* analysis, was used. Quantitative real-time PCR (qPCR) was performed using a ABI 7500 real-time PCR system (Applied Biosystems) and SYBR GreenER qPCR SuperMix Universal (Invitrogen). Primers for qPCR were: *Ca_V1A*: 5′-ACTCGACCAAAGATTATCAATCCGAT-3′, 5′-CCACCAAACATTTGCATACCAAGAAG-3′; *Ca_V1B*: 5′-CTTTCAAAGAAGATTACAGTGGCACA-3′, 5′-ACCAAACTCGGTATCTGAAACTCTGTT-3′; *Ca_V2A*: 5′-TACGATGGAAGGGTGGACAGATGTT-3′,5′-AAGCTCGTCTTTTCTCTACTCTTTCTC-3′; *β-actin*: 5′-GGTAATGAACGATTTAGATGTCCAGAAG-3′, 5′-TCTGCATACGATCAGCAATACCTGGAT-3′; *wnt-1*: 5′-ATCGCACAGGATTGGTTGTTGCT-3′,5′-GTTCCATAATTGTTTTCGATCTCGT-3′; *wnt11-5*: 5′-TTGGTGTCAGACATCAAGGATTTCA-3′,5′-GCCTTGACAGTTCCAAACGTGGTT-3′. In all cases, at least one qPCR primer was localized outside the sequence of the RNAi construct. For absolute qPCR analyses, cDNA (not containing the RNAi targeted sequence) for each construct was cloned into pGEM-T Easy vector (Promega) and used as a template to create gene-specific standard curves for assessing mRNA levels in samples isolated at equivalent regenerative timepoints from different worms. The mRNA levels of specific genes was compared with controls using *D. japonica β-actin* to normalize RNA input. As a further calibration of absolute qPCR results, data were compared to those from a semi-quantitative RT-PCR analysis of the same sample (data not shown).

Confocal Ca^{2+} imaging and $^{45}Ca^{2+}$ assays—Dissociated planarian cells were obtained by cutting worms into ~10 fragments in Ca^{2+}-free Holtfreter's solution (5/8 dilution) supplemented with 1mM EDTA, 1% BSA (w/v) and 1% FBS (v/v). Fragments were washed in Ca^{2+}-free Holtfreter's (5/8) and dissociated to single cells by incubation in 0.25% (w/v) trypsin for 15 minutes at room temperature, pipetting periodically with a Pasteur pipette. Enzymatic digestion was arrested with the addition of 10% (v/v) FBS and the dissociated cells were filtered though a 40 μm nylon mesh, followed by centrifugation (7mins, 300 x g). Cells were resuspended to a density of approximately 10^6 cells/ml. For Ca^{2+} imaging, dissociated cells were plated onto poly-D-lysine coated 35mm petri dishes (MatTek) and stored at room temperature for 18-24 hours. Adhered cells were loaded with fluo4-AM (90mins, 4μM) in Ca^{2+}-free Holtfreter's (5/8) containing 2% BSA (w/v) and 0.025% pluronic, and then washed in Holtfreter's (5/8) supplemented with Ca^{2+} (1mM) for 30 minutes prior to imaging. Dishes were imaged using an Andor Revolution spinning disc confocal microscope and changes in fluorescence monitored (λ_{ex}=488nm, λ_{em}=525nm) following addition of either PZQ or vehicle controls. Fractionation of the crude dissociation sample was performed by serial centrifugation (10mins at 100 x g, 200 x g, 1000 x g, 3000 x g, 14,000 x g sequentially), such that the supernatant of each centrifugation step was removed and spun at increasing speeds to separate fractions by size. Fractions were fixed (8% paraformaldehyde in PBS), stained with a NeuroTrace green fluorescent Nissl stain

(Invitrogen, 1:100 dilution in PBS, 40mins), and counterstained in DAPI (1μg/ml, 10mins). For $^{45}Ca^{2+}$ experiments, intact cells were incubated in Ca^{2+}-containing Holtfreter's (5/8) solution (1mM Ca^{2+} supplemented with $^{45}Ca^{2+}$ (9μCi/ml)) in the absence or presence of various concentrations of PZQ (100nM-100μM). After 30 minutes, cells were harvested by filtration in ice-cold sucrose-citrate solution (GF/B, Whatman) using a Brandel Harvester (Marchant et al, 1997) and cellular $^{45}Ca^{2+}$ uptake assessed by liquid scintillation counting. Protein was quantified by Bradford assays for normalization of data between different fractions.

RESULTS

We serendipitously discovered that trunk fragments of the planarian *Dugesia japonica* exposed to the drug praziquantel (PZQ) immediately after amputation regenerated as viable, two-headed animals (Figure 1A) with dual integrated central nervous systems (Nogi et al, 2009). The effect was highly penetrant (94±4% bipolar, 70μM PZQ for 48hrs) and the duplication of the CNS by external drug application was clearly shown by *in situ* hybridization of a CNS marker (Figure 1A). Mechanistic explanation of this effect is lacking: notably, the *in vivo* target(s) of PZQ remain unresolved despite its usage as a clinical drug for over 30 years (Day et al, 1992; Cioli and Pica-Mattoccia, 2003; Caffrey, 2007). Prior *in vitro* evidence has implicated several possible molecular targets (Wiest et al, 1992; McTigue et al, 1995; Tallima and El Ridi, 2007; Angelucci et al, 2007; Gnanasekar et al, 2009), including activation of Ca^{2+} influx in muscle (Pax et al, 1978; Kohn et al, 2001a), however the *in vivo* relevance of such pathways has not been determined owing to a lack of functional genetic data. Our initial data – (i) PZQ increased $^{45}Ca^{2+}$ uptake, (ii) bipolarity was phenocopied by depolarization and (iii) attenuated by either the L-type Ca^{2+} channel antagonist nicarpidine or (iv) RNAi of accessory $Ca_v\beta$ subunits (Nogi et al, 2009) – was supportive of the Ca^{2+} hypothesis and justified analysis of a requirement for specific Ca_v channels. However, the lack of any molecular data about the Ca^{2+} channels themselves precluded such analysis, despite the fact the striking duplication of the CNS achieved by PZQ exposure provided a simple visual screen for RNAi analysis of molecules needed for PZQ efficacy *in vivo*.

Planarian Ca_v channels

To enable a candidate RNAi approach, we characterized the entire family of planarian voltage-operated Ca^{2+} channel α ($Ca_v\alpha$) subunits. Five discrete $Ca_v\alpha$ subunits[1] were identified using degenerate PCR (Figure 1B). Four subunits displayed high similarity to high voltage activated $Ca_v\alpha$ subunits (HVA, Figure 1B), two of which clustered with vertebrate L-type $Ca_v\alpha$ channels (christened *Ca_v1A* and *Ca_v1B*) and two with non-L type sequences (*Ca_v2A* and *Ca_v2B*). The remaining $Ca_v\alpha$ subunit most closely resembled a T-type subunit (*Ca_v3*), representing the first low-voltage activated (LVA) $Ca_v\alpha$ subunit reported in flatworms. Compared with established invertebrate models which express only single representatives from the three $Ca_v\alpha$ gene families (EGL-19, UNC-2, CCA-1 in *C. elegans* (Yeh et al, 2008); Dmca1D, Dmca1A, and Ca-α_{1T} in *Drosophila* (King, 2007)), the molecular repertoire of $Ca_v\alpha$ subunits in planarians was clearly more expansive.

As a first step toward investigating physiological roles for individual $Ca_v\alpha$ subunits, we focused on the two Ca_v1 subunits (*Ca_v1A* and *Ca_v1B*). Full length sequences for *Ca_v1A* and *Ca_v1B* encoded proteins of 1812 (Ca_v1A) and 2652 (Ca_v1B) amino acids such that Ca_v1B potentially represents the largest HVA Ca^{2+} channel identified to date in any species (Zheng

[1]**GENBANK Accession Numbers**: *Dugesia japonica* Ca_V1A (HQ724315), Ca_V1B (HQ724316), Ca_V2A (HQ724317), Ca_V2B (HQ724318), Ca_V3(HQ724319), APC (HQ738520), βcatenin-1 (HQ738521), *wnt11-5* (HQ738522), *wnt1* (HQ738523).

et al, 1995). Each Ca_v1 subunit possessed an architecture characteristic of the voltage-gated ion channel superfamily, comprising four repeated domains (I-IV) of 6 transmembrane spanning helices (S1-S6) with overall high sequence homology (Figure 1B & 2). Diagnostic Ca_v features included: (i) a re-entrant P-loop, located between S5 and S6, harbouring the conserved glutamic acid residue that contributes to the EEEE selectivity gate in all HVA $Ca_v\alpha$ subunits; (ii) essential residues within the alpha-interacting domain between domain I and II that are crucial for $Ca_v\beta$ interaction, and (iii) the isoleucine-glutamine (IQ) domain, $preIQ_3$ domain and EF-hand consensus motifs within the cytoplasmic COOH terminus that mediate Ca^{2+}-regulation of L-type Ca_v channels. Despite this architectural similarity, the functional properties of planarian Ca_v channels are likely unique from their vertebrate counterparts. For example, a definitive pharmacology of vertebrate Ca_v1 channels is modulation by dihydropyridines. A critical methionine residue for dihydropyridine binding in IIIS6 that is found in Ca_v1 channels from rat (M1161 in $\alpha 1_C$) as well as *C. elegans* (M1056 in EGL-19) was represented by isoleucine in both the *D. japonica* Ca_v1 subunits (Figure 2). Having been isolated as a resistant polymorphism (M1056I) toward nemadipine-evoked growth retardation in *C. elegans* (Kwok et al, 2008), this isoleucine substitution likely confers dihydropyridine insensitivity to the *D. japonica* Ca_v1 subunits. Therefore, extrapolation of pharmacological and regulatory properties from vertebrate Ca_v subtypes to their planarian orthologues is unsupported from overall sequence homology, which never surpassed 50% identity (Table 1).

Unique roles of Ca_v1 subunits

In vivo RNAi was used to investigate whether Ca_v1 subunit function impacted PZQ-evoked bipolarity. RNAi constructs targeting multiple regions of *Ca_v1A* and *Ca_v1B* were designed and worms were fed bacteria expressing dsRNA against individual *$Ca_v\alpha$* subunits (Sánchez Alvarado and Newmark, 1999). Constructs serving as phenotypically positive (*Dj-six-1*, a transcription factor required for eye regeneration (Mannini et al, 2004)) and negative RNAi controls (*Smed-six-1*, the same gene from *Schmidtea mediterranea* but with no phenotypic outcome owing to sequence divergence) were included in each assay. The RNAi protocol comprised two dual feeding and regenerative cycles, lasting ~1 month in total duration (Figure 3A). Prior to the final regenerative cycle, a cohort of worms was removed for real time PCR analysis to assess gene knockdown at the point of assaying the bipolarizing effect of PZQ. This protocol permitted screening individual RNAi constructs for optimal effectiveness and selectivity: *Ca_v1A* mRNA were decreased by ~60% with no significant change in *Ca_v1B* mRNA; *Ca_v1B* proved more resistant to knockdown - levels of mRNA were decreased by ~30% but with only a 4% change in Ca_v1A levels in the same samples (Figure 3B).

Following *Ca_v1* subunit RNAi, the effectiveness of PZQ in evoking bipolarity was evaluated. PZQ induced two-headed worms with high efficacy in the positive phenotype (eyeless) control cohort (*Dj-six-1*, 80±8%), the negative (RNAi) control cohort (*Smed-six-1*, 82±5%) and naïve worms (82±3% with 90μM PZQ for 24hrs). In contrast, *Ca_v1A* knockdown markedly antagonized the bipolarizing ability of PZQ (Figure 3C), with ~3-fold fewer bipolar regenerants in *$Ca_v1A(RNAi)$* worms compared with controls (Figure 3D). Bipolar worms occurred in high numbers with *$Ca_v1B(RNAi)$* worms, and moreover the penetrance of this effect (96±2%, n=6 trials) appeared greater than controls ($p<0.05$, Figure 3D). Given the difficulty of confirming potentiation to such a high dose of PZQ, we repeated these experiments using a lower PZQ concentration (50μM, 24hrs) such that both decreases and increases in bipolar worm numbers could be easily assayed.

In this suppressor-enhancer screen, all trunk fragments from RNAi control and naïve worms regenerated with normal head-tail polarity in the absence of PZQ (Figure 3E), whereas the lower dose of PZQ produced a smaller proportion of two-headed worms (30±2%, n=5 trials) as expected. Surprisingly, knockdown of the two discrete *Ca_V1* isoforms produced different effects on PZQ-evoked bipolar regeneration. Knockdown of *Ca_V1A* again attenuated the anteriorization effect of PZQ (16±2%, n=4 trials; Figure 3E) whereas RNAi of *Ca_V1B* increased the number of bipolar regenerants (83±4%, n=4 trials), a ~2.8-fold potentiation over the control cohort (Figure 3E). The opposing effects of Ca_v1A and Ca_v1B on PZQ-evoked bipolarity were not mimicked by knockdown of at least one other Ca_v isoform. RNAi targeting *Ca_V2A* (Nogi et al, 2009), which resulted in a ~60% decrease in *Ca_V2A* mRNA, did not substantially change the proportion of PZQ-evoked two-headed worms (25±2%, n=4 trials) relative to controls (29±2%, n=5 trials). Therefore, RNAi targeting of three different $Ca_v\alpha$ subunits yielded three different outcomes (Ca_v1A, attenuation, Ca_v1B, potentiation; Ca_v2A, no effect) on PZQ-evoked bipolarity.

If PZQ acts to activate voltage-operated Ca^{2+} entry, then other depolarizing stimuli should also effect anteriorization. Therefore, we analyzed the effects of elevated [K^+] (by 30mM, a sufficient depolarizing stimulus in flatworms (Novozhilova et al, 2010)) in both control and *Ca_V(RNAi)* worms (Figure 3F). Elevated [K^+] yielded only a few two-headed worms in control and *Ca_V1A(RNAi)* worms (9±4% and 3±2%, respectively). However a majority of *Ca_V1B(RNAi)* worms displayed bipolar regeneration (56±7%) with the same treatment. First, these data show that *Ca_V1* RNAi differentially miscued regenerative polarity in response to PZQ (Figure 3D&E) or depolarization (Figure 3F). Second, the contrast between the effectiveness of PZQ and K^+ exposure in control worms was noteworthy: PZQ produced two-headed worms with high effectiveness in control worms (Figure 3D&E), whereas depolarization alone was a far less effective stimulus (Figure 3F). These data suggest selectivity in PZQ action on a subset of $Ca_v\alpha$ subunits (Ca 1A), compared to elevated K^+ v acting as a non-selective depolarizing stimulus on a population of Ca^{2+} channels with opposing functions (Ca_v1A versus Ca_v1B).

A simple model based on RNAi data is shown in Figure 3G. The key feature is the opposing roles of Ca_v1A and Ca_v1B. Consistent with Ca_v1B knockdown potentiating the number of two-headed worms produced by PZQ and K^+ treatments (Figure 3), as well as the formation of a smaller number of bipolar regenerants during normal regeneration (2.4±0.7%, Figure 3E&F), Ca_v1B is assigned to function in a posteriorization pathway. Consistent with *Ca_V1A* RNAi blocking PZQ efficacy (Figure 3), PZQ likely activates Ca_v1A and this effect is likely selective for Ca_v1A over Ca_v1B on account of the different penetrance of PZQ versus K^+ as depolarizing cues. The assignment of Ca_v1A in a pathway antagonistic to Ca_v1B function is also consistent with the observation of a cohort of *Ca_V1A(RNAi)* worms with inhibited head regeneration (2.2±0.7%, n=5 trials). This simple scheme provides a conceptual framework to define how voltage-gated Ca^{2+} entry modulates regenerative outcomes.

PZQ activates Ca^{2+} influx via Ca_v1A in a neuronally-enriched cell fraction

In what cell type(s) are the Ca_v1 channels active in planaria? There exists surprisingly little knowledge about the cellular physiology of different planarian cell types, likely due to the lack of cell culturing methods since differentiated cells do not divide (neoblasts are the only mitotically active cells). Therefore, to address this question, we performed confocal Ca^{2+} imaging experiments in acutely dissociated samples prepared from entire worms. Planaria were dissociated into a heterogenous cell mixture that was plated on glass-bottomed dishes for confocal imaging. In samples loaded with the high affinity Ca^{2+} indicator fluo-4 (K_d for Ca^{2+} ~345nM), addition of PZQ resulted in an increase in fluorescence in a subset of cells (Figure 4A). Analysis of time-resolved fluorescence ratios from responding cells revealed that PZQ (100μM), but not vehicle controls, evoked a rapid Ca^{2+} transient (F/F_0 = 2.75±0.5, n=18 cells).

To obtain large quantities of this subpopulation, we performed fractionation experiments to isolate the responsive cells. Serial centrifugation experiments determined this fraction was wellseparated from larger cells simply by centrifugation at higher speeds (Figure 4B). Centrifugation yielded discrete 'heavy' (centrifugation , <300 x g for 5 mins) and 'light' (centrifugation >300 x g for 5 mins) fractions for analysis, with the latter containing the responsive population identified in the single cell Ca^{2+} imaging assays. Notably, the 'light' fractions stained positively with a NeuroTrace (Nissl) stain, with little staining in the 'heavy' fraction (Figure 4B). Therefore both the size and staining profile suggested the responsive fraction was neuronally-derived (Morita and Best, 1966; Best and Noel, 1969). $^{45}Ca^{2+}$ uptake experiments were then performed on both the 'heavy' and 'light' fractions to compare the efficacy of PZQ in both fractions. Increasing concentrations of PZQ evoked a progressive uptake of $^{45}Ca^{2+}$ in cells present within the 'light' fraction (EC_{50}=0.98μM). The extent of $^{45}Ca^{2+}$ entry was significantly smaller (~4-fold) in the 'heavy' fraction sample, underscoring the initial observation made by Ca^{2+} imaging (Figure 4A) that PZQ activates Ca^{2+} entry into a discrete subset of planarian cells.

Having optimized the population-level $^{45}Ca^{2+}$ assay, it was possible to compare results in different RNAi backgrounds. On the basis of the RNAi data implying PZQ activates Ca_v1A (Figure 3F), we compared $^{45}Ca^{2+}$ uptake in control RNAi (*Smed-six-1*) and Ca_v1A RNAi backgrounds in response to PZQ. Submaximal PZQ (1μM) failed to enhance $^{45}Ca^{2+}$ uptake over control levels in Ca_v1A RNAi worms, in contrast to the increase observed in control RNAi worms. Similarly, $^{45}Ca^{2+}$ uptake evoked by a maximal concentration of PZQ (50μM) was inhibited by Ca_v1A RNAi. The inhibition of PZQ-evoked Ca^{2+} entry by Ca_v1A knockdown in response to PZQ supports the interpretation of RNAi data (Figure 3F) to suggest PZQ activates Ca^{2+} entry via Ca_v1A.

Ca_v1 channels modulate early patterning decisions

Where does Ca^{2+} act to miscue regeneration? Recently, immense progress has been made in elucidating signaling events regulating planarian regeneration. The crucial breakthrough was identification of a βcatenin isoform in *Schmidtea mediterranea* (*Smed-βcatenin-1*) essential for posterior (tail) specification during regeneration, likely by controlling transcriptional activation of a posterior fate circuit. Knockdown of *Smed-βcatenin-1* yielded animals with head structures that regenerated from each wound (Iglesias et al, 2008; Petersen and Reddien, 2008; Gurley et al, 2008).

To probe the locus of action of PZQ, we compared two-headed phenotypes resulting from either pharmacological or genetic treatments. Both PZQ exposure and *βcatenin-1* RNAi yielded two-headed animals with high penetrance (~90%) from regenerating trunk fragments (Figure 5A). For PZQ, this occurred over a single regeneration cycle and reflected a rapid and complete remodeling of the entire anterior-posterior (AP) axis. This entailed duplication of the pharynx and anteriorization of gut structures within the regenerating trunk, in addition to regeneration of the dual, integrated CNS and head structures from the blastema (Figure 5B). For *βcatenin-1(RNAi)* animals, the penetrance of the bipolar phenotype in the population increased more gradually over time, as knockdown was effected over several feeding/regeneration cycles (Figure 5A). To assess whether these pharmacological (PZQ) and genetic [*βcatenin-1* RNAi] pathways to bipolarity were independent we performed an enhancement screen using a low dose of PZQ and a sub-penetrant RNAi feeding cycle, either alone or in combination (Figure 6). Low dose PZQ or sub-optimal *βcatenin-1* RNAi produced a low percentage of two-headed worms after regeneration (9±5% and 20±7%, respectively; Figure 6). However, in combination, the same treatments produced many bipolar worms (80±4%; Figure 6), a proportion ~2.8-fold larger than simple additivity of bipolar percentages from the individual treatments. This synergism between PZQ and *βcatenin-1* RNAi treatments implied mechanistic convergence in their actions. We conclude

PZQ acts rapidly via inhibitory interactions with Wnt signaling events that control AP polarity through βcatenin-1 (Figure 6), but not as a direct inhibitor of βcatenin-1 itself owing to the phenotypic divergence between the different bipolarity inducing treatments (Figure 5B).

An alternative to analysis of dual anteriorizing cues is evaluation of antagonism between PZQ and posteriorizing signals. The intractability of transgenic methods in planarians precluded a gain of function approach (e.g. *βcatenin-1* overexpression). Rather such analyses must be realized via RNAi of inhibitors of posteriorization circuits to potentiate 'tail' signaling indirectly. In the context of Wnt signaling, APC - a physiological inhibitor of βcatenin stability - provides such a target. *APC* RNAi yielded two-tailed animals regenerating from trunk fragments (Figure 7A), consistent with the logic that knockdown of *APC* elevates βcatenin-1 (Gurley et al, 2008). The two-tailed worms displayed impaired movement, and owing to the lack of CNS coordination of the feeding response, were viable for only ~1 month. Co-treatment of *APC* RNAi worms with PZQ (70μM for 24hrs) resulted in a high proportion of two-tailed worms (94±4% two-tailed worms, n=3, Figure 7A). This contrasted with PZQ exposure in *Smed-six1* RNAi worms, or naïve worms which produced a high proportion of two-headed worms under identical conditions (Figure 7A). Lengthening the duration of PZQ exposure to 2 or even 3 days failed to inhibit the two-tailed phenotype observed in *APC(RNAi)* worms (Figure 7A). These data suggest APC impacts anterior-posterior patterning downstream of the target of PZQ, as PZQ treatment is unable to overcome the effects of *APC* RNAi.

Recent experiments have implicated Hedgehog (Hh) signaling as an upstream transcriptional regulator of Wnt expression in planarians (Yazawa et al, 2009; Rink et al, 2009). If PZQ acts upstream of canonical Wnt signaling events, does PZQ-evoked Ca^{2+} entry impact Hh signaling? To test this, we applied similar logic (knockdown of an inhibitor of posteriorization) to examine the effects of knockdown of *patched* (*ptc*), an endogenous inhibitor of the Hh signaling module. Knockdown of *Dj-ptc* posteriorized regeneration (35±3%, worms with two-tails or inhibited head), a low penetrance compared with *APC* RNAi but consistent with modulation of an upstream modulator (Yazawa et al, 2009). Different from results with *APC* RNAi, PZQ treatment of *ptc(RNAi)* worms blocked the formation of two-tailed worms (Figure 7A). In contrast, knockdown of Hh, the physiological ligand and upstream component of *ptc*, resulted in a small percentage of two-headed worms (3.1±0.7%, n=3 trials) and treatment of *Hh* RNAi worms with PZQ mimicked results seen with control cohorts at longer time periods (Figure 7A). The ability of PZQ to suppress bipolar tail formation in *ptc(RNAi)* worms supports a modulation of Hh signaling components by voltage-operated Ca^{2+} influx, upstream of canonical Wnt signaling (Figure 7F).

If the logic that PZQ impacts Hh signaling is correct, then PZQ should modulate the levels of mediators that serve as the output of Hh signaling events. Hh signaling regulates the transcription of Wnt genes - notably *wnt1*, a wound-induced Wnt that activates βcatenin-1 during tail regeneration, and the downstream effector *wnt11-5* (Figure 7F, (Adell et al, 2009; Petersen and Reddien, 2009; Gurley et al, 2010)). Crucially, loss of Hh signaling activity (via RNAi) inhibits *wnt1* expression (Yazawa et al, 2009; Rink et al, 2009). Therefore, if PZQ inhibits Hh signaling, *wnt1* expression should be reduced.

Consequently, we performed qPCR analysis of *wnt1* in trunk and posterior blastema samples. Relative to control samples, regenerating trunk samples exposed to PZQ showed a decrease in *wnt1* and *wnt11-5* levels (Figure 7B). Resolution of the time course of changes in *wnt1* and *wnt11-5* in the posterior blastema after amputation revealed that PZQ exposure attenuated the early wound-induced increase in *wnt1* expression (~12-18hrs, Figure 7C) that occurs prior to determination of polarity (i.e. preceding changes in *wnt11-5*, Figure 7D). Therefore, PZQ is impacting *wnt* levels at a timeframe causative, rather than consequent of polarity specification (Petersen and Reddien, 2009). Further, *in situ* hybridization patterns of *wnt1* and *wnt11-5* during trunk fragment regeneration were compared to samples treated with PZQ. *wnt1* and *wnt11-5* expression was reduced by PZQ with similar kinetics to qPCR results (Figure 7E). As PZQ evoked changes in *wnt1* intensity precede changes in *wnt11-5*, these data are consistent with the conclusion that PZQ is impacting early events. Finally, as Wnt/βcatenin signaling maintains AP axis polarity in intact worms (Gurley et al, 2008; Petersen and Reddien, 2008; Iglesias et al, 2008), we were also interested in determining whether PZQ modulated Wnt expression during normal body homeostasis. In intact worms, *wnt1* and *wnt11-5* expression was also decreased by PZQ exposure (data not shown). Therefore, both qPCR and *in situ* hybridization approaches demonstrated that PZQ decreased *wnt1* expression, consistent with early inhibition of the *Hh* signalling module by PZQ.

We have previously shown that PZQ-evoked Ca^{2+} entry is inhibited by RNAi of Ca_v1A (Figure 4D). If PZQ-evoked changes in *wnt1* were also dependent on Ca^{2+} entry via Ca_v1A then RNAi of Ca_v1A channels should attenuate the PZQ-evoked decrease in *wnt1*. Therefore, we performed qPCR analysis of both *wnt1* and *wnt11-5* in *Ca_v1A(RNAi)* and *Ca_v1B(RNAi)* worms, compared to RNAi controls (*Smed-six-1(RNAi)*). Whereas PZQ treatment resulted in decreased levels of *wnt1* and *wnt11-5* in the control RNAi cohort, knockdown of Ca_v1A prevented any PZQ-evoked decrease in either *wnt1* or *wnt11-5* (Figure 8). In contrast, PZQ treatment was still effective at causing a decrease in *wnt1* and *wnt11-5* in *Ca_v1B(RNAi)* worms. We conclude that RNAi of Ca_v1A, but not Ca_v1B, prevents PZQ-evoked Ca^{2+} entry and PZQ-evoked inhibition of *wnt1* and *wnt11-5*.

Nervous system expression of Ca_v channels and Hh signaling machinery

The conclusion that PZQ inhibited Hh signaling implied a spatial relationship between Ca_v channels and the Hh signaling machinery. *In situ* analysis of *Ca_v1A* and *Ca_v1B* localization in intact worms revealed *Ca_v1A* was predominantly expressed in brain as well as pharynx, whereas *Ca_v1B* was confined to the central nervous system with expression in the brain and ventral nerve cords (Figure 9A). Expression of Ca_v1 isoforms in the nervous system was also evident from analysis of *Ca_v1* staining in regenerating trunk fragments. *Ca_v1A* and *Ca_v1B* were detected in regenerating brain tissue at the anterior blastema by 18hrs after amputation (Figure 9B), at the same time point as the earliest known anterior markers. These data do not preclude a later role of Ca^{2+} channels in the development of anterior structures (Beane et al. 2011) in addition to their earlier role in modulating Hh signaling after injury (Figures 7&8). This neuronal localization of both Ca_v1 isoforms is therefore consistent with the cell physiological data resolving PZQ-evoked Ca^{2+} influx in a neuronally-derived cell population (Figure 4). Crucially, an antisense probe against *Hh* was also found to stain the central nervous system (Figure 9A, (Rink et al, 2009;Yazawa et al, 2009)). Therefore the demonstration that *Ca_v1A*, *Ca_v1B* and *Hh* are all expressed within the planarian nervous system, further supports the regulatory interplay between voltage-operated Ca^{2+} entry and Hh signaling.

DISCUSSION

The planarian model holds great appeal for neuroscientists interested in studying the wholescale regeneration of a nervous system (Cebrià, 2007). The experimental system is simple and increasingly tractable (Newmark and Sanchez-Alvarado, 2002; Reddien et al, 2005; Robb et al, 2008; Chan and Marchant, 2011), yet the endpoint is complex in terms of structure (Morita and Best, 1966; Mineta et al, 2003), gene-expression profiles (Cebrià et al, 2002), neurotransmitter diversity (Ribeiro et al, 2005; Collins et al, 2010) and potential for behavioral insight (Kitamura et al, 2003; Raffa et al, 2003).

Our interest relates to the use of this system to identify small molecules efficacious *in vivo* at modulating stem cell behavior. Indeed, the utility of invertebrate models for studying conserved mechanisms of stem cell regulation is increasingly appreciated (Brand and Livesey, 2011). We previously discovered that agents disrupting cellular Ca^{2+} homeostasis anteriorized regeneration, with PZQ (a drug of unknown mechanism of action) being exceedingly effective at producing worms with dual, integrated nervous systems (Nogi et al, 2009). Here, by identifying a family of planarian $Ca_v\alpha$ subunits we provide chemical genetic data that PZQ activates a specific Ca_v1 isoform (Ca_v1A) to miscue regeneration by inhibiting Hh signaling. Knockdown of Ca_v1A prevented PZQ-evoked anteriorization (Figure 3), PZQ-evoked Ca^{2+} entry (Figure 4) and the PZQ-evoked decrease in *wnt1* (Figure 8), the output of neuronally-derived Hh signaling (Yazawa et al, 2009; Rink et al, 2009). The significance of these data are two-fold. First, they establish a unique interplay between specific Ca_v channels isoforms and Hedgehog signaling in the control of stem cell differentiation, that on the basis of recently published data appears also relevant to vertebrates. Second, they provide *in vivo* support for PZQ efficacy being dependent on neuronal Ca_v isoforms of discrete subunit composition.

Ca_v channels and neuronal stem cell differentiation

Unbiased *in vitro* screens have uncovered new, and existing, activators of voltage-operated Ca^{2+} influx that regulate the differentiation and proliferation of various multipotent stem cells (Schneider et al, 2008; Wang et al, 2009). In the context of neurogenesis, application of Ca_v1 agonists to proliferating neuronal stem cells in culture enhances neuronal fate (Deisseroth et al, 2004; D'Ascenzo et al, 2006; Diamandis et al, 2007; Schneider et al, 2008). By extending such findings to a model suited for studying pluripotent cells *in vivo*, our data demonstrate a novel role for voltage-operated Ca^{2+} entry in regulating wholescale nervous system regeneration. The observed anteriorization of regenerative responses by PZQ-evoked Ca^{2+} entry is reminiscent of proposed roles for voltage-operated Ca^{2+} entry in neurogenesis and neural induction in vertebrate models (Leclerc et al, 1997; Webb and Miller, 2003; Deisseroth et al, 2004; Whitaker, 2006), and the consequent Ca^{2+}-dependent inhibition of Hh signals supportive of an emerging literature showing reciprocal interplay between morphogens and Ca_v1 channel activity. Examples include Wnts (which can both activate Ca_v1 channels (Panákova et al, 2010), and serve as transcriptional effectors of neuronal voltage-operated Ca^{2+} entry (Alvania et al, 2006)), as well as noggin and FGF signals that regulate Ca_v activity during neural induction (Moreau et al, 2008; Lee et al, 2009). Therefore, our findings underscore a fundamental and evolutionary conserved role for voltage-operated Ca^{2+} influx controlling stem cell differentiation, and the utility of basic invertebrate models for studying neural stem cell biology (Brand and Livesey, 2011). Characterization of planarian Ca_v channels revealed a surprisingly diverse family of $Ca_v\alpha$ subunits compared to better studied invertebrate models (Figure 1B). This diversity is likely a general characteristic of flatworms: first, four HVA $Ca_v\alpha$ subunits are predicted in the *Schistosoma mansoni* genome (Kohn et al, 2001b; Berriman et al, 2009); second, each of the subunits described here has a clearly identifiable homolog within the *Schmidtea mediterranea* genome (Robb et al, 2008). The Ca_v channel diversity was functionally significant, rather than reflecting redundant gene duplication, as the two Ca_v1 family isoforms differentially regulated regenerative outcomes. RNAi of *Ca_v1A* blocked bipolar regeneration, whereas *Ca_v1B* RNAi increased the number of two-headed regenerants whether in the absence of drug, or from PZQ or K^+ exposure (Figure 3). The surprising different roles for Ca^{2+} influx through Ca_v1 isoforms (Ca_v1A versus Ca_v1B) explains previous observations that established activators and inhibitors of Ca_vs can both yield

NIH-PA Author Manuscript
NIH-PA Author Manuscript

bipolar worms, albeit with different penetrances (Nogi et al, 2009). Differential selectivity of pharmacological agents for Ca_v1 isoforms with opposing roles likely underpins these observations, and highlight the possibility that small molecule neurogenics can encompass compounds acting as either selective activators (Ca_v1A) or inhibitors (Ca_v1B) of Ca_v channels *in vivo*. Data suggesting differences in pharmacophore binding profiles to specific neuronal Ca_v1 channel isoforms is significant in this regard for future development of Ca_v1 subtype specific neurogenic compounds (Sinnegger-Brauns et al, 2009).

Finally, pharmacological profiling of the neuronal flatworm $Ca_v\alpha$ subunits is extremely important in the context of defining the molecular site of action of PZQ. PZQ is the mainstay therapeutic for combating Schistosomiasis, a parasitic flatworm disorder that infects over 200 million people worldwide (Day et al, 1992; Cioli and Pica-Mattoccia, 2003; Caffrey, 2007). However, the relevant *in vivo* target(s) of this clinically important drug have remained undefined for decades, hampering rational design of new antischistosomal agents that target the same vulnerable pathways in the parasite. Our data are significant in this regard by first, narrowing PZQ efficacy to Ca^{2+} channel complexes of specific $Ca_v\alpha$ composition (Ca_v1A) and second, by suggesting a revised focus on a neuronal rather than a muscular site(s) of action of PZQ.

Ca^{2+} regulation of Hh signaling

During planarian regeneration, Hh is the most upstream activator of neoblast differentiative responses following wounding (Yazawa et al, 2009; Petersen and Reddien, 2009). Hh evoked changes in *wnt1* and *wnt11-5* expression occur in a stem cell independent manner (Yazawa et al, 2009; Petersen and Reddien, 2009), such that initial *wnt1* and *wnt11-5* expression occurs even in irradiated worms (Petersen and Reddien, 2009). In vertebrates also, the Hedgehog system acts as a paracrine regulator of stem cell behavior in normal proliferative scenarios, and as an aberrant pathway in cancer (Varjosalo and Taipale, 2007; Yauch et al, 2008; Traiffort et al, 2010). In the CNS, Shh release has been proposed to maintain an adult neurogenic niche and regulate the proliferation of neuronal precursors in different brain regions (Traiffort et al, 2010). Our demonstration of regulation of Hh signaling by PZQ-evoked voltage-operated Ca^{2+} entry establishes a largely unrecognized functional interaction between two signaling systems which individually are highly competent at nuclear reprogramming and crucial for central nervous system development (Whitaker, 2006; Greer and Greenberg, 2008; Traiffort et al, 2010). Is the regulatory interplay demonstrated between these signaling pathways in planaria conserved in vertebrate systems? Although PZQ efficacy is unique to the flatworm system (as is ideal for a selective therapeutic), the principle of Ca_v regulation of Hedghehog signaling appears conserved on the basis of two recently published studies.

First, cytoplasmic Ca^{2+} signals have been shown to act as downstream effectors of Sonic hedgehog (Shh) signaling in *Xenopus* embryonic neurons (Belgacem and Borodinsky, 2011). By imaging the neural tube of developing frog embryos, Ca^{2+} spike activity trended with the Shh gradient crucial for dorsalventral patterning of the spinal cord. Shh failed to increase Ca^{2+} spike activity when Ca_vs were blocked (Belgacem and Borodinsky, 2011). Such data place Ca^{2+} as a downstream effector of Hh activity, a coupling that may also exist in stem cells and other cell types (Osawa et al, 2006; Heo et al, 2007). This observation is entirely consistent with our data showing Ca_v1A regulation of the Hh signaling module at, or downstream of, Ptc (Figure 7). None-the-less, the specific Hh signaling components that are regulated by Ca^{2+}, and the customization of this regulation between different systems, remain to be elucidated. However, the demonstration that PZQ activates a Ca_v1 channel to inhibit Hh transcriptional effects is highly reminiscent of the paradigm that Ca_v1 silencing is needed to support activity-dependent gene expression in certain vertebrate neurons (Chang and Berg, 2001).

Second, recent evidence from various neuronal cell types has shown that Shh is sorted to the regulatory secretory pathway in axons and is available for release by depolarization (Beug et al, 2011). The demonstration of a link between Ca_v channels and Hh signaling suggest an obvious connection between neuronal activity, Ca_v activation and synaptic Hh secretion that may be important for both maintaining progenitors and regulating their proliferation. In planaria, Ca_v1B likely fulfills this role by regulating neuronal Hh release to ensure normal posterior patterning. As *Hh* is predominantly localized to the planarian nervous system, it is likely that neuronal damage on amputation releases Hh to the surrounding environment effecting the *wnt1* wound response. Continued delivery of Hh to posterior wounds through the ventral nerve cords has been suggested (Yazawa et al, 2009) to stabilize posterior-specification mechanisms dependent on *βcatenin-1* and *wnt11-5*. Loss of Ca_v1B function would therefore increase anteriorization outcomes (Figure 3) by repression of depolarization-evoked Hh release.

In summary, our data establish a unique regulatory interplay between specific Ca_v1 isoforms and Hh signals that control planarian nervous system regeneration *in vivo*. This is demonstrated by activation of Ca_v1A by the antischistosomal drug PZQ, casting new light on the relevant *in vivo* mechanism of action of this important clinical agent

Acknowledgments

We thank Dr. J. S. Hwang and Dr. T. Gojobori (National Institute of Genetics, Japan) for provision of an EST clone (BP191017). Work in the lab is supported by NSF (MCB0919933) and NIH (GM088790).

References

Adell T, Salo E, Boutros M, Bartscherer K. Smed-Evi/Wntless is required for ß-catenin-dependent and -independent processes during planarian regeneration. Development. 2009; 136:905–910. [PubMed: 19211673]

Alvania RS, Chen X, Ginty DD. Calcium Signals Control Wnt-Dependent Dendrite Growth. Neuron. 2006; 50:813–815. [PubMed: 16772162]

Angelucci F, Basso A, Bellelli A, Brunori M, Mattoccia L Pica, Valle C. The antischistosomal drug praziquantel is an adenosine antagonist. Parasitol. 2007; 134:1215–1221.

Beane WS, Morokuma J, Adams DS, Levin M. A chemical genetics approach reveals H,K-ATPase-mediated membrane voltage is required for planarian head regeneration. Chem Biol. 2011; 18:77–89. [PubMed: 21276941]

Belgacem YH, Borodinsky LN. Sonic hedghog signaling is decoded by calcium spike activity in the developing spinal cord. Proc Natl Acad Sci USA. 2011; 108:4482–4487. [PubMed: 21368195]

Berriman M, Haas BJ, LoVerde PT, Wilson RA, Dillon GP, Cerqueira GC, Mashiyama ST, Al-Lazikani B, Andrade LF, Ashton PD, Aslett MA, Bartholomeu DC, Blandin G, et al. The genome of the blood fluke *Schistosoma mansoni*. Nature. 2009; 460:352–360. [PubMed: 19606141]

Best JB, Noel J. Complex synaptic configurations in planarian brain. Science. 1969; 164

Beug ST, Parks RJ, McBride HM, Wallace VA. Processing-dependent trafficking of Sonic hedgehog to the regulatory secretory pathway in neurons. Mol Cell Neuro. 2011; 46:583–596.

Brand AH, Livesey FJ. Neural stem cell biology in vertebrates and invertebrates: more alike than different? Neuron. 2011; 70:719–29. [PubMed: 21609827]

Caffrey CR. Chemotherapy of schistosomiasis: present and future. Curr Op Chem Biol. 2007; 11:433–439.

Cebrià F. Regenerating the central nervous system: how easy for planarians. Dev Genes Evol. 2007; 217:733–748. [PubMed: 17999079]

Cebrià F, Kudome F, Nakazawa M, Mineta K, Ikeo K, Gojobori T, Agata K. The expression of neural-specific genes reveals the structural and molecular complexity of the planarian central nervous system. Mech Dev. 2002; 116:199–204. [PubMed: 12128224]

Chan JD, Marchant JS. Pharmacological and Functional Genetic Assays to Manipulate regeneration of the Planarian *Dugesia japonica*. JoVE. 2011 doi 10.3791/3058.

Chang KT, Berg DK. Voltage-gated channels block nicotinic regulation of CREB phosphorylation and gene expression in neurons. Neuron. 2001; 32:855–865. [PubMed: 11738031]

Cioli D, Pica-Mattoccia L. Praziquantel. Parasitol Res. 2003; 90:S3–S9. [PubMed: 12811543]

Collins JJ, Hou X, Romanova EV, Lambrus BG, Miller CM, Saberi A, Sweedler JV, Newmark PA. Genome-wide analyses reveal a role for peptide hormones in planarian germline development. PLoS Biology. 2010; 8:e10000509.

D'Ascenzo M, Piacentini R, Casalbore P, Budoni M, Pallini R, Azzena GB, Grassi C. Role of L-type Ca^{2+} channels in neuronal stem/progenitor differentiation. Eur J Neurosci. 2006; 23:935–944. [PubMed: 16519658]

Day TA, Bennett JL, Pax RA. Praziquantel: the enigmatic antiparasitic. Parasitol Today. 1992; 8:324–4.

Deisseroth K, Singla S, Toda H, Monje M, Palmer TD, Malenka RC. Excitation-neurogenesis coupling in adult neural stem/progenitor cells. Neuron. 2004; 42:535–52. [PubMed: 15157417]

Diamandis P, Wildenhain J, Clarke ID, Sacher AG, Graham J, Bellows DS, Ling EKM, Ward RJ, Jamieson LG, Tyers M, Dirks PB. Chemical genetics reveals a complex functional ground state of neural stem cells. Nat Chem Biol. 2007; 3:268–273. [PubMed: 17417631]

Fredlander MR, Adamidi C, Han T, Lebedeva S, Isenbarger TA, Hirst M, Marra M, Nusbaum C, Lee WL, Jenkin JC, Sánchez Alvarado A, Kim JK, Rajewsky N. High-resolution profiling and discovery of planarian small RNAs. Proc Natl Acad Sci USA. 2009; 106:11546–11551. [PubMed: 19564616]

Gnanasekar M, Salunkhe AM, Mallia AK, He YK, Kalyanasundaram R. Praziquantel affects the regulatory myosin light chain of Schistosoma mansoni. Antimicrob Agents Chemother. 2009; 53:1054–60. [PubMed: 19104008]

Greer PL, Greenberg ME. From Synapse to Nucleus: Calcium-Dependent Gene Transcription in the Control of Synapse Development and Function. Neuron. 2008; 59:846–860. [PubMed: 18817726]

Gurley KA, Elliott SA, Simakov O, Schmidt HA, Holstein TW, Sánchez Alvarado A. Expression of secreted Wnt pathway components reveals unexpected complexity of the planarian amputation response. Dev Biol. 2010; 347:24–39. [PubMed: 20707997]

Gurley KA, Rink JC, Sánchez-Alvarado A. β-catenin defines head versus tail identity during planarian regeneration and homeostasis. Science. 2008; 319:323–7. [PubMed: 18063757]

Heo JS, Lee MY, Han HJ. Sonic Hedgehog Stimulates Mouse Embryonic Stem Cell Proliferation by Cooperation of Ca^{2+}/Protein Kinase C and Epidermal Growth Factor Receptor As Well as Gli1 Activation. Stem Cells. 2007; 25:3069–3080. [PubMed: 17901397]

Iglesias M, Gomez-Skarmeta JL, Saló E, Adell T. Silencing of *Smed-βcatenin1* generates radial-like hypercephalized planarians. Development. 2008; 135:1215–1221. [PubMed: 18287199]

King GF. Modulation of insect Ca_v channels by peptidic spider toxins. Toxicon. 2007; 49:513–30. [PubMed: 17197008]

Kitamura Y, Inden M, Sanada H, Takata K, Taniguchi T, Shimohama S, Orii H, Mochii M, Agata K, Watanabe K. Inhibitory effects of antiparkinsonian drugs and caspase inhibitors in a parkinsonian flatworm model. J Pharmacol Sci. 2003; 92:137–142. [PubMed: 12832841]

Kohn AB, Anderson PAV, Roberts-Misterly JM, Greenberg RM. Schistosome calcium channel β subunits. UNUSUAL MODULATORY EFFECTS AND POTENTIAL ROLE IN THE ACTION OF THE ANTISCHISTOSOMAL DRUG PRAZIQUANTEL. J Biol Chem. 2001a; 40:36873–36876.

Kohn AB, Lea JM, Roberts-Misterly JM, Anderson PAV, Greenberg RM. Structure of three high voltage-activated calcium channel α1 subunits from *Schistosoma mansoni*. Parasitol. 2001b; 123:489–497.

Kwok TCY, Hui K, Kostelecki W, Ricker N, Selman G, Feng Z-P, Roy PJ. A genetic screen for dihydropyridine (DHP)-resistant worms reveals new residues required for DHP-blockage of mammalian calcium channels. PLoS Genetics. 2008; 4:e10000067.

Leclerc C, Daguzan C, Nicolas M-T, Chabret C, Duprat A-M, Moreau M. L-type calcium channel activation controls the in vivo transduction of the neuralizing signal in the amphibian embryos. Mech Dev. 1997; 64:105–110. [PubMed: 9232601]

Lee KW, Moreau M, Néant I, Bibonne A, Leclerc C. FGF-activated calcium channels control neural gene expression in *Xenopus*. Biochim Biophys Acta. 2009:1033–1040. [PubMed: 19135096]

Mannini L, Rossi L, Deri P, Gremigni V, Salvetti A, Salo E, Batistoni R. *Djeyes absent* (*Djeya*) controls prototypic planarian eye regeneration by cooperating with the transcription factor *Djsix-1*. Dev Biol. 2004; 269:346–359. [PubMed: 15110705]

Marchant JS, Beecroft MD, Riley AM, Jenkins DJ, Marwood RD, Taylor CW, Potter BVL. Disaccharide polyphosphates based upon adenophostin A activate hepatic D-*myo*-inositol 1,4,5-trisphosphate receptors. Biochemistry. 1997; 36:12780–12790. [PubMed: 9335535]

McTigue MA, Williams DR, Tainer JA. Crystal structures of a schistosomal drug and vaccine target: Glutathione S-transferase from *Schistosoma japonica* and its complex with the leading antischistosomal drug praziquantel. J Mol Biol. 1995; 246:21–27. [PubMed: 7853399]

Mineta K, Nakazawa M, Cebria F, Ikeo K, Agata K, Gojobori T. Origin and evolutionary process of the CNS elucidated by comparative genomics analysis of planarian ESTs. Proc Natl Acad Sci USA. 2003; 100:7666–71. [PubMed: 12802012]

Moreau M, Neant I, Webb SE, Miller AL, Leclerc C. Calcium signalling during neural induction in *Xenopus laevis* embryos. Phil Trans R Soc B. 2008; 363:1371–1375. [PubMed: 18198153]

Morita M, Best JB. Electron microscopic studies of planaria. III. Some observations on the fine structure of planarian nervous tissue. J Exp Zool. 1966; 161:391–411. [PubMed: 5959741]

Newmark PA, Sanchez-Alvarado A. Not your father's planarian: a classic model enters the era of functional genomics. Nat Rev Genet. 2002; 3:210–219. [PubMed: 11972158]

Nogi T, Zhang D, Chan JD, Marchant JS. A Novel Biological Activity of Praziquantel Requiring Voltage-Operated Ca^{2+} Channel β subunits: Subversion of Flatworm Regenerative Polarity. PLoS NTD. 2009; 3:e464.

Novozhilova E, Kimber MJ, Qian H, McVeigh P, Robertson AP, Zamanian M, Maule AG, Day TA. FMRFamide-Like Peptides (FLPs) Enhance Voltage-Gated Calcium Currents to Elicit Muscle Contraction in the Human Parasite *Schistosoma mansoni*. PLoS NTD. 2010; 4:e790.

Osawa H, Ohnishi H, Takano K, Noguti T, Mashima H, Hoshino H, Kita H, Stato K, Matsui H, Sugano K. Sonic hedgehog stimulates the proliferation of rat gastric mucosal cells through ERK activation by elevating intracellular calcium concentration. BBRC. 2006; 344:680–687. [PubMed: 16630542]

Panákova D, Werdich AA, MacRae CA. Wnt11 patterns a myocardial electrical gradient through regulation of the L-type Ca^{2+} channel. Nature. 2010; 466:874–878. [PubMed: 20657579]

Pax R, Bennett JL, Fetterer R. A benzodiazepine derivative and praziquantel: effects on musculature of *Schistosoma mansoni* and *Schistosoma japonicum*. Archives Pharmacol. 1978; 304:309–315.

Petersen CP, Reddien PW. Smed-*βcatenin-1* is required for anteroposterior blastema polarity in planarian regeneration. Science. 2008; 319:327–330. [PubMed: 18063755]

Petersen CP, Reddien PW. A wound-induced Wnt expression program controls planarian regeneration polarity. Proc Natl Acad Sci USA. 2009; 106:17061–6. [PubMed: 19805089]

Raffa RB, Stagliano GW, Umeda S. κ-opioid withdrawal in Planaria. Neurosci Lett. 2003; 349:139–142. [PubMed: 12951188]

Reddien PW, Bermange AL, Murfitt KJ, Jennings JR, Sánchez Alvarado A. Identification of genes needed for regeneration, stem cell function, and tissue homeostasis by systematic gene perturbation in planaria. Dev Cell. 2005; 8:635–649. [PubMed: 15866156]

Ribeiro P, El-Shehabi F, Patocka N. Classical transmitters and their receptors in flatworms. Parasitol. 2005; 131:S19–S40.

Rink JC, Gurley KA, Elliott SA, Alvarado AS. Planarian Hh signaling regulates regeneration polarity and links Hh pathway evolution to cilia. Science. 2009; 326:1406–1410. [PubMed: 19933103]

Robb SMC, Ross E, Sanchez Alvarado A. SmedGD: the Schmidtea mediterranea genome database. Nuc Acid Res. 2008; 36:D599–606.

Sánchez Alvarado A, Newmark PA, Robb SM, Juste R. The Schmidtea mediterranea database as a molecular resource for studying platyhelminthes, stem cells and regeneration. Development. 2002; 129:5659–65. [PubMed: 12421706]

Schneider JW, Gao Z, Li S, Farooqi M, Tang TS, Bezprozvanny I, Frantz DE, Hsieh J. Small-molecule activation of neuronal cell fate. Nat Chem Biol. 2008; 4:408–410. [PubMed: 18552832]

Sinnegger-Brauns MJ, Huber IG, Koschak A, Wild C, Obermair GJ, Einzinger U, Hoda JC, Sartori SB, Striessnig J. Expression and 1,4-dihydropyridine-binding properties of brain L-type calcium channel isoforms. Mol Pharm. 2009; 75:407–414.

Sánchez Alvarado A, Newmark PA. Double-stranded RNA specifically disrupts gene expression during planarian regeneration. Proc Natl Acad Sci USA. 1999; 96:5049–5054. [PubMed: 10220416]

Tallima H, El Ridi R. Praziquantel binds *Schistosoma mansoni* adult worm actin. Int J Antimicrob Agents. 2007; 29:570–5. [PubMed: 17341443]

Traiffort E, Angot E, Ruat M. Sonic Hedgehog signaling in the mammalian brain. J Neurochem. 2010; 113:576–590. [PubMed: 20218977]

Varjosalo M, Taipale J. Hedgehog Signaling. J Cell Sci. 2007; 120:3–6. [PubMed: 17182898]

Wang W, Walker JR, Wang X, Tremblay MS, Lee JW, Wu X, Schultz G. Identification of small-molecule inducers of pancreatic ß-cell expansion. Proc Natl Acad Sci USA. 2009; 106:1427–1432. [PubMed: 19164755]

Webb SE, Miller AL. Calcium signaling during early embryonic development. Nat Rev Mol Cell Biol. 2003; 4:539–551. [PubMed: 12838337]

Whitaker M. Calcium at fertilization and in early development. Phys Rev. 2006; 86:25–88.

Wiest PM, Li Y, Olds R, Bowen WD. Inhibition of phosphoinositide turnover by praziquantel in *Schistosoma mansoni*. J Parasitol. 1992; 78:753–755. [PubMed: 1321906]

Yauch RL, Gould SE, Scales SJ, Tang T, Tian H, Ahn CP, Marshall D, Fu L, Januario T, Kallop D, Nannini-Pepe M, Kotkow K, Marsters JC Jr. Rubin LL, de Sauvage FJ. A paracrine requirement for hedgehog signalling in cancer. Nature. 2008; 455:406–411. [PubMed: 18754008]

Yazawa S, Umesono Y, Hayashi T, Tarui H, Agata K. Planarian Hedgehog/Patched establishes anterior-posterior polarity by regulating Wnt signaling. Proc Natl Acad Sci USA. 2009; 106:22329–22334. [PubMed: 20018728]

Yeh E, Ng S, Zhang M, Bouhours M, Wang Y, Wang M, Hung W, Aoyagi K, Melnik-Martinez K, Li M, Liu F, Schafer WR, Zhen M. A putative cation channel, NCA-1, and a novel protein, UNC-80, transmit neuronal activity in C. elegans. PLoS Biol. 2008; 6:e55. [PubMed: 18336069]

Zheng W, Feng G, Ren D, Eberl DF, Hannan F, Dubald M, Hall LM. Cloning and characterization of a calcium channel alpha 1 subunit from Drosophila melanogaster with similarity to the rat brain type D isoform. J Neurosci. 1995; 15:1132–1143. [PubMed: 7869089]

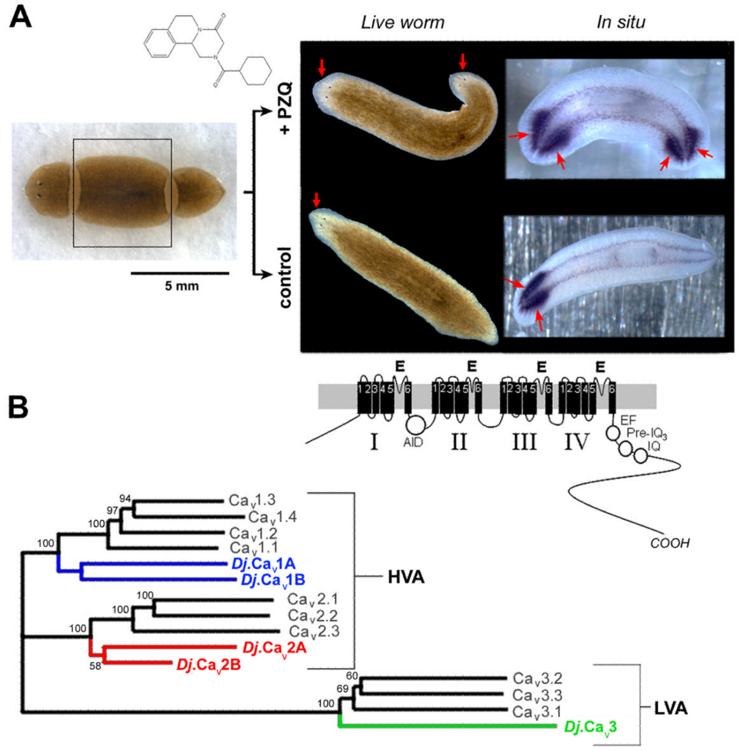

Figure 1. PZQ-evoked bipolarity and characterization of planarian $Ca_v\alpha$ subunits

(A) *Left*, Overview of regenerative assay. Trunk fragment (boxed) was isolated and incubated with PZQ (structure, top) in samples to be compared with control worms (*bottom*). *Right*, Images of bipolar worms (head, arrowed) produced after PZQ exposure (*top*) in live worms (*left*) and samples stained for the CNS marker PC2 (*right*). Control worms are shown for comparison (*bottom*). **(B)** Phylogenetic analysis of sequence homology between planarian and human $Ca_v\alpha$ sequences aligned using MUSCLE and displayed as an unrooted tree assembled by a neighbor joining algorithm (Geneious 5.0). Bootstrap values are indicated at nodes. The lower value for *D. japonica* Ca_v2 subunits relates to the use of partial sequences. Accession numbers are referenced in Table 1, with addition of $Ca_v2.1$ (O00555), $Ca_v2.2$ (Q00975), $Ca_v3.2$ (O95180) and $Ca_v3.3$ (Q9P0X4). The *D. japonica* subunit previously referred to as $Ca_v1.1$(Nogi et al, 2009) is renamed Ca_v2A to standardize nomenclature with the *Schistosome* literature (Kohn et al, 2001b). *Inset*, schematic of Ca_v1 architecture (domains I-IV) and motifs (alpha-interaction domain, AID; EF-hand motif, EF; pre-IQ_3 and IQ motif).

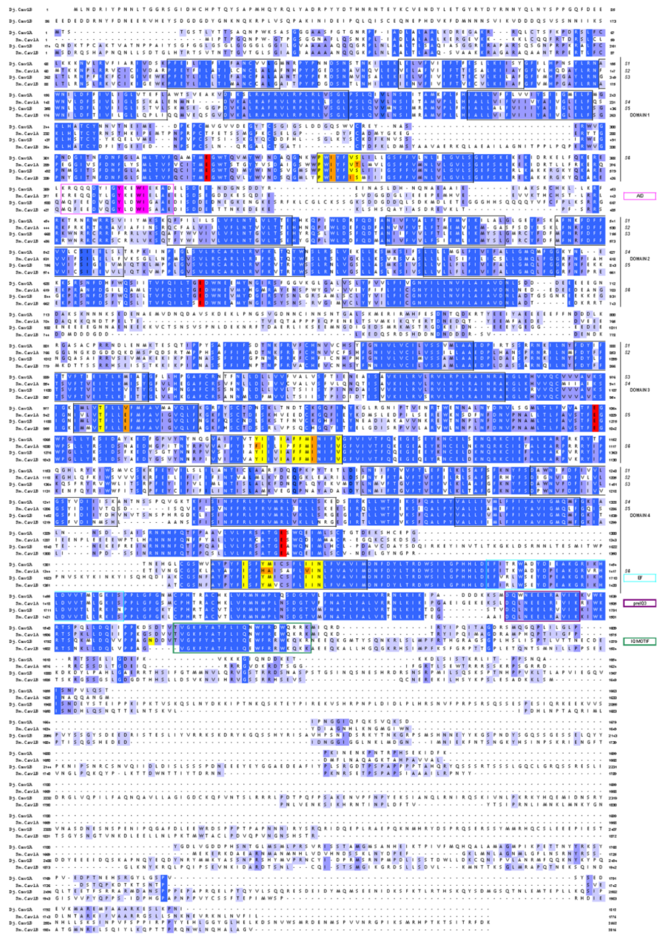

Figure 2. Sequence alignment of flatworm Ca_v1 subunits

Sequence alignment of *Dugesia japonica* Ca_v1A (*Dj*-Ca_v1A) and Ca_v1B (*Dj*-Ca_v1B) with *Schistosoma mansoni* Ca_v1A (*Sm*.Ca_v1A, AF361884) and Ca_v1B (*Sm*.Ca_v1B, CAZ34413.1). Sequences were aligned in Jalview using MUSCLE. Features were assigned with reference to a rat brain $Ca_v1.2$ subunit (Genbank #AAA18905) and indexed in the right hand column. These include highlighted residues that illustrate conservation of key residues within the α-interaction domain (AID, magenta), the EEEE ion selectivity filter motif (red), cytoplasmic COOH-terminal EF (blue), preIQ3 (purple) and IQ (green) regulatory domains, as well as twenty residues required for dihydropyridine interaction that are identical (yellow) or divergent (orange) in flatworm Ca_v sequences from rat $Ca_v1.2$ sequence. The isoleucine residue present in flatworm Ca_v1 subunits that may be relevant to DHP sensitivity is found as residue I1106 in Ca_v1A and I1317 in Ca_v1B.

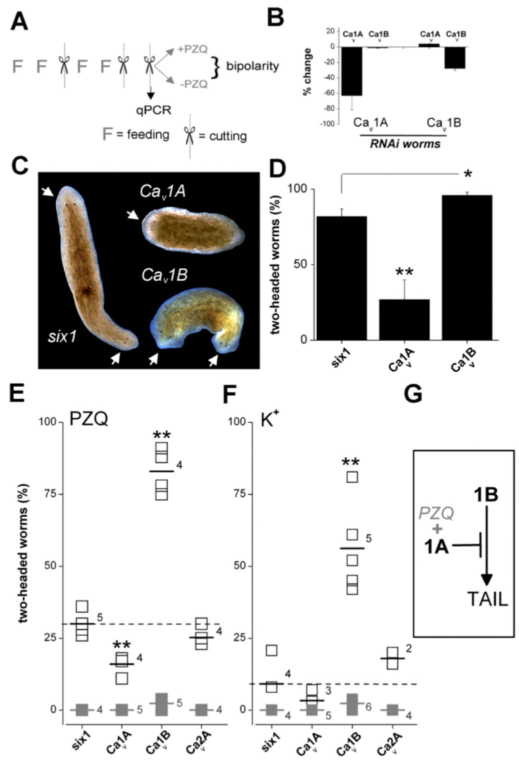

Figure 3. RNAi of Ca_V1 subunits modulates bipolar regeneration

(A) Protocol for *in vivo* RNAi. Two cycles of dual feeding (F) and regeneration (scissors) were followed by a regenerative assay in the presence or absence of PZQ. Bipolarity was scored 7 days after the final regeneration. A cohort of trunk fragments was removed prior to drug exposure to assess the effectiveness and specificity of ablation of individual mRNAs at the time of drug addition using qPCR. All RNAi assays followed this protocol (FFxFFxx) with exceptions of *APC* (FFFFx), *Ptc* (FFFFxFFFx) and *Hh* (FFFxFFxx). (**B**) Assessment of changes in mRNA abundance for *Ca_V1* subunits in worms fed either *Ca_V1A(RNAi)* or *Ca_V1B(RNAi)* constructs respectively. **(C)** Images showing bipolar worms (head, arrowed) regenerating in *Smed-six-1* and *Ca_V1B*, but not *Ca_V1A* cohorts . **(D)** Percentage of two-headed worms in *Smed-six-1* (control), *Ca_V1A* or *Ca_V1B* cohorts following exposure to PZQ (90μM for 24hrs). For clarity only the *Smed-six-1* control cohort is shown – similar results were obtained in naïve and *Dj-six-1* worms (see text). Asterisks indicate probability of similarity at $p<0.05$ (*) and $p<0.01$ (**). **(E)** Two-headed regenerants in the absence (grey, solid) or presence (black, open) of a lower dose of PZQ (50μM for 24hrs) in *six-1* (control), *Ca_V1A* or *Ca_V1B* worms. Numbers report the number of independent trials, and short horizontal lines indicate the arithmetic mean of these experiments. Dashed line indicates mean value of control (*six-1*) dataset. **(F)** Effect of depolarizing conditions. Trunk fragment regeneration in media with elevated $[K^+]$ (supplemented by 30mM, 24hrs). PZQ was not present in these assays. **(G)** Working model for Ca_V1 channels in regenerative polarity.

NIH-PA Author Manuscript
NIH-PA Author Manuscript
NIH-PA Author Manuscript

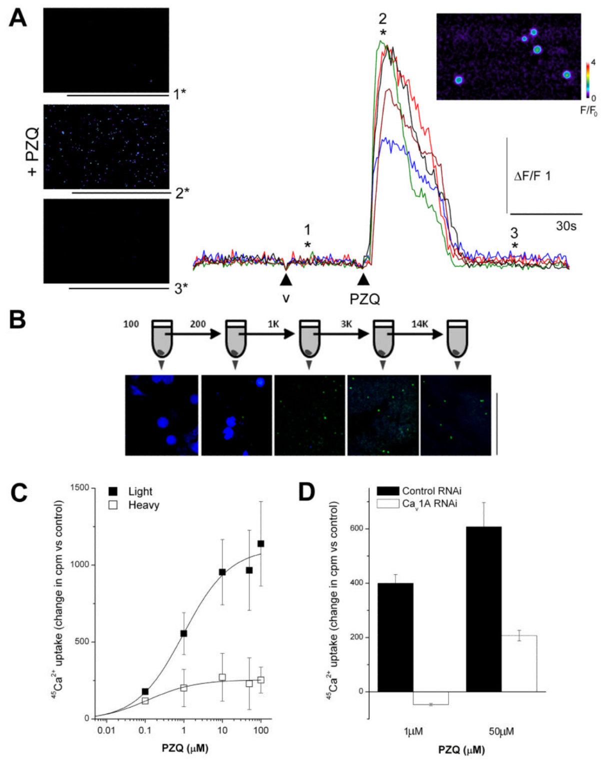

Figure 4. PZQ activates Ca^{2+} entry via Ca_v1A channels

(A) *Left*, Confocal Ca^{2+} imaging of dissociated planarian cells depicting fluo-4 fluorescence on application of control vehicle (image '1'), as well as during ('2') and after ('3') application of PZQ (100μM). *Right*, traces show fluorescence profiles from five discrete cells, with the timepoints of images as indicated (v = vehicle). *Inset*, Higher magnification image of responsive cells from which fluorescence profiles were collected (position '2*'). Fluo-4 fluorescence is represented on a pseudocolor scale where increasing warm coloration represents greater fluorescence emission. Fluorescence (F), and change in fluorescence (ΔF) is calibrated relative to fluorescence at time=0 (F_0). **(B)** Schematic of serial centrifugation protocol. The dissociated planarian suspension was first spun at 100 x g to yield a pellet, which was retained for staining, while the supernatant was spun at the next higher speed. This procedure was repeated up to a final step at 14,000 x g. The constituents of the pellet was visualized at each stage using DAPI (blue) and NeuroTrace (green), scalebar = 50μm. **(C)** Comparison of $^{45}Ca^{2+}$ uptake in response to increasing concentrations of PZQ in equivalent 'light' (solid) and 'heavy' fraction samples (open) in the same preparation. **(D)** Ca_v1A RNAi inhibited absolute $^{45}Ca^{2+}$ uptake in response to submaximal (1μM) and maximal (50μM) concentrations of PZQ. Data are generated from the 'light' fraction and expressed relative to untreated samples from the same preparative fractionation.

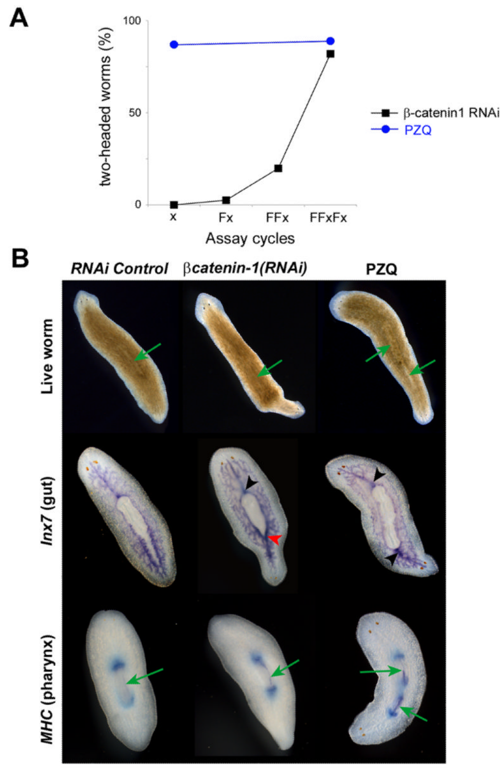

Figure 5. Comparison of genetic and pharmacological routes to bipolarity

(A) Number of two-headed worms produced by pharmacological (70μM PZQ, 24hrs) or knockdown methods [(*Dj-βcatenin-1(RNAi)*] at indicated number of feeding (F) and regeneration (x) cycles from a representative experiment. **(B)** Images of live worms (top) and *in situ* hybridization staining of gut (*Inx7*, middle) and pharyngeal (MHC, bottom row) markers in regenerating worms in control (control RNAi, left), PZQ treated (70μM for 24hrs; imaged after 7 days; right) and worms subject to RNAi of *βcatenin-1* (middle, 7 days). In *βcatenin-1(RNAi)* worms, the bipolar conversion occurred more slowly than with PZQ exposure. Newly anteriorized structures appeared to emerge from the posterior regenerative blastema without immediate remodeling of tissues within the trunk fragment. *In situ* hybridization of gut and pharyngeal marker after 14 days did not show clear evidence of full duplication unlike the effects elicited by PZQ. Rather, AP remodeling occurred over time in *βcatenin-1(RNAi)* worms subsequent to the emergence of head structures, in a manner reminiscent of intercalation events as seen in grafting experiments. Green arrows indicate the pharynx in live worms (top). Black arrowhead highlights a typical single anterior gut branch connecting with the pharynx. Red arrowhead indicates a gut organization intermediate between the normal anterior and posterior morphology.

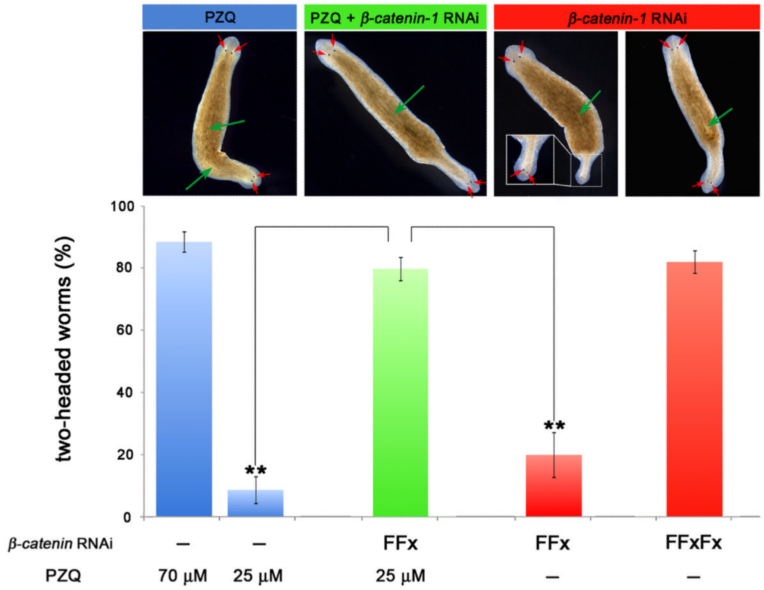

Figure 6. PZQ and βcatenin-1 knockdown act synergistically to anteriorize regeneration

Analysis of the interaction between drug (PZQ) and genetic [*βcatenin-1(RNAi)*] routes to bipolarity. Graph details the percentage of two-headed worms resulting from treatments with high (70μM) or low dose PZQ (25μM for 24hrs, blue) compared with optimal (multiple feeding and regeneration cycles) and suboptimal RNAi of *βcatenin-1* (two feedings and single regeneration cycle, red). Treatment of worms subject to suboptimal *βcatenin-1(RNAi)* with low dose PZQ is shown in green. Images show phenotypes associated from drug treatments (blue), *βcatenin-1* knockdown (red), and dual treatments (green). The two images for *βcatenin-1(RNAi)* are representative of results from the suboptimal (left) and optimal (right) RNAi protocol.

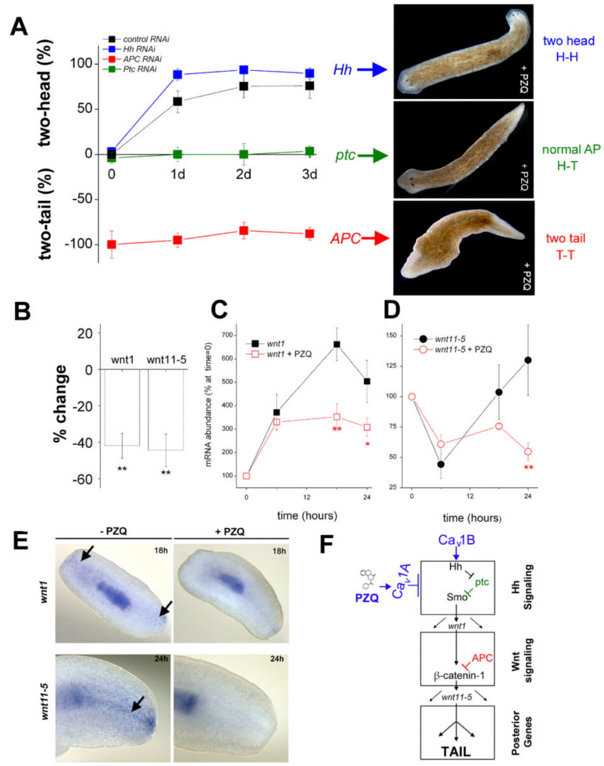

Figure 7. Inhibitory interaction of PZQ-evoked Ca^{2+} influx with Hh/Wnt signaling pathway

(A) Left, chemical genetic screen of PZQ efficacy in naïve (open squares) and different cohorts of RNAi worms, including negative RNAi control (black), *Hh* (blue) *APC* (red) and *Ptc* (green) RNAi. The duration of PZQ exposure (90μM) is shown on the abscissa, and the resulting bipolarity (two-headed, normal, two-tailed) shown on the ordinate. Right, representative images of dominant phenotype for *Hh*, *Ptc* and *APC* RNAi worms exposed to PZQ.**(B)** qPCR data of changes in *wnt1* and *wnt11-5* levels in regenerating trunk fragments exposed to PZQ (90μM, 24hrs) relative to untreated controls. **(C)** qPCR analysis of *wnt1* mRNA levels in the posterior blastema at indicated times after amputation (at t=0) in the absence (black) and presence of PZQ (red squares, 90μM). Asterisks indicate probability of similarity at $p<0.05$ (*) and $p<0.01$ (**)**. (D)** Similar qPCR analysis for *wnt11-5* levels. **(E)** *In situ* hybridization of *wnt1* and *wnt11-5* (arrowed) in the absence and presence of PZQ (90μM) in regenerating trunk fragments at indicated times. (**F**) Schematic of signaling modules involved in anterior-posterior specification. At least two distinct signal transduction pathways – Hedgehog (top) and Wnt signaling (middle) modules – control AP specification during regeneration as evidenced by RNAi of individual components of each module. These modules culminate to impact levels of βcatenin-1, which regulate a posterior fate circuit. Our data demonstrate an interaction of PZQ-evoked Ca^{2+} influx via Ca_v1A with Hh/Wnt signaling (top), localized upstream to APC within the Hh signaling module. Ca_v1B likely inhibits the trafficking/release of Hh from neurons (see Discussion).

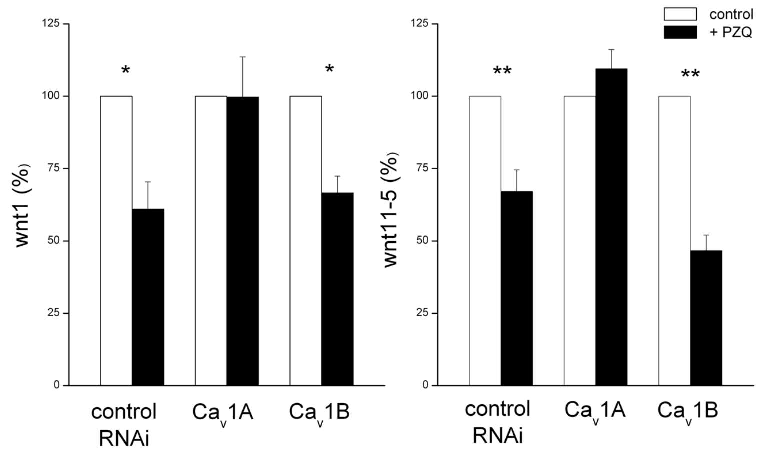

Figure 8. NAi of Ca_v1A blocks PZQ-evoked changes in *wnt* mediators

qPCR analysis of **(A)** *wnt1* and **(B)** *wnt11-5* levels in posterior blastema samples from different cohorts of RNAi worms (*Smed-six-1* RNAi worms, Ca_v1A and Ca_v1B RNAi worms) isolated after 24hrs of regeneration in the absence (open) or presence (solid) of PZQ (70μM). Difference from controls indicated at $p<0.01$ (**) and $p<0.05$ (*)

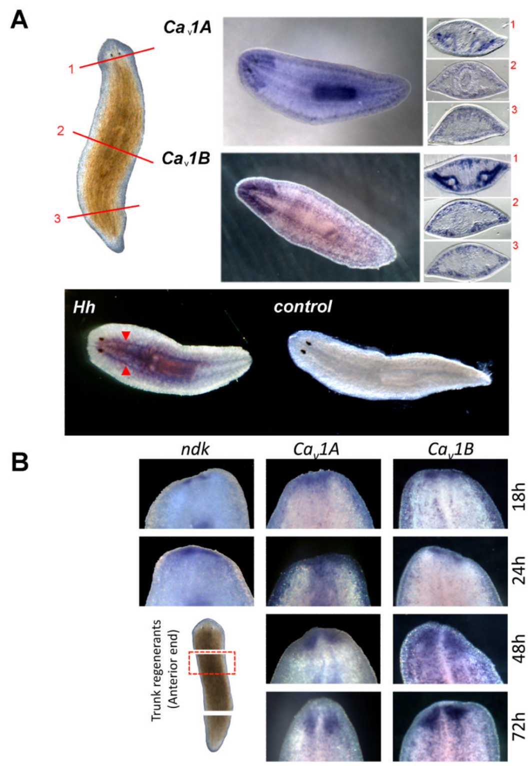

Figure 9. Localization of Ca_V1 channels with Hh in the planarian nervous system

(**A**) *Top*, *Ca_V1A* and *Ca_V1B* localization in whole mount and sectioned samples. Brightfield image of intact planarian shows location of cross sections: anterior (1, top), pharyngeal (2, middle) and post-pharyngeal (3, bottom). Sections are orientated with the ventral side at the bottom. *Bottom*, whole mount *in situ* hybridization of *Hh* showing localization of mRNA within the ventral nerve cords (red arrows) compared with controls. (**B**) Whole mount *in situ* hybridization of *ndk* (a brain marker), *Ca_V1A* and *Ca_V1B* in the anterior blastema during trunk fragment regeneration at the indicated times.

Table 1

Comparison of flatworm and vertebrate $Ca_V\alpha$ identity.

		Dj Ca_v1A	*Dj* Ca_v1B	*Sm* Ca_v1A	*Sm* Ca_v1B	*Sm* Ca_v2A	*Hs* Ca_v1.1	*Hs* Ca_v1.2	*Hs* Ca_v1.3	*Hs* Ca_v1.4	*Hs* Ca_v2.3	*Hs* Ca_v3.1
Ca_v1	*Dj* Ca_v1A		52%	57%	54%	39%	49%	48%	49%	48%	38%	23%
	Dj Ca_v1B			50%	61%	34%	49%	46%	47%	48%	37%	22%

Sequences were aligned using the BLOSUM62 scoring matrix (ClustalW MSA), and amino acid identities computed. *Sm*.Ca_V1 was renamed *Sm*.Ca_V1A, owing to the *in silico* predication of a second Ca_V1 subunit in *Schistosoma mansoni* (named *Sm*.Ca_V1B, Genbank #CAZ34413.1). Subunits for which complete coding sequences have been biologically verified are shown in bold. Shading highlights groupings with the highest identity, and different species are boxed. The following accession numbers were used: *Schistosoma mansoni* (*Sm*): *Sm*.Ca_V1A (AF361884), *Sm*.Ca_V1B (CAZ34413.1), *Sm*.Ca_V2A (AF361883); *Homo sapiens* (*Hs*): *Hs*.Ca_V1.1 (Q13698), *Hs*.Ca_V1.2 (Q13936), *Hs*.Ca_V1.3 (Q1668), *Hs*.Ca_V1.4 (O60840), *Hs*.Ca_V2.3 (Q15878), *Hs*.Ca_V3.1 (O43497).